ALL-SOLID-STATE ION-SELECTIVE SENSORS FOR MEASUREMENT OF POTASSIUM IONS IN AQUEOUS MEDIA

BY

IHDA USWATUN SHALIHAH BINTI SHOHIBUDDIN

A thesis submitted in fulfillment of the requirement for the degree of Master of Science (Electronics Engineering)

Kulliyyah of Engineering
International Islamic University Malaysia

FEBRUARY 2022

ABSTRACT

Ion-selective electrode (ISE) sensors have been widely used in diagnostics, food security, and environmental monitoring applications owing to their low-cost and straightforward fabrication processes. However, monitoring physiological ions in real-time remains a challenge where conventional ISEs suffer poor sensitivity, limit of detection, and lifetime due to the sensing membranes of conventional ISEs, where ions were not efficiently converted into electrons. Therefore, this project aims to utilize nanomaterials of poly(3,4-ethylenedioxythiophene):polystyrenesulfonate as all-solid-state transducers to improve the sensitivity, limit of detection, and lifetime of the sensor. Moreover, this work aims to develop all-solid-state potassium ion-selective electrode (AS-K^+ISE) sensors for detection and quantification of potassium ions (K^+) in aqueous media. This research is also to evaluate and validate the sensor performance of the AS-K^+ISE sensors by monitoring dynamic K^+ changes in aedes mosquito larvae. The effects of modifying low-cost screen-printed carbon electrodes (SPCEs) with poly(3,4-ethylenedioxythiophene):polystyrenesulfonate (PEDOT:PSS), reduced graphene oxide stabilized in polystyrenesulfonate (rGO:PSS), and their composite (rGO:PSS-PEDOT:PSS) on the electrical conductivity and electrochemical reversibility of electrochemical sensor performance were characterised in terms of peak current (I_p), peak-to-peak potential separation (ΔE_p), shift in peak potentials (E_{p_shift}), and effective surface area (A_e). Cyclic voltammetry (CV) results revealed transducer rGO:PSS-PEDOT:PSS has synergistic effect of PEDOT:PSS and rGO:PSS, where PEDOT:PSS has high peak current (I_p) suggesting fast electron transfer kinetics at the electrode-electrolyte interface, and rGO:PSS is reversible as evidenced by small ΔE_p and E_{p_shift}. Owing to PEDOT:PSS having the highest peak current of 1.637 mA which is 23 folds higher than rGO:PSS, AS-K^+ISE sensors were fabricated by drop-casting potassium-selective membrane (KISM) onto PEDOT:PSS/SPCEs. Potentiometry measurements were used to determine limit of detection, sensitivity, linear range, lifetime, response time, and selectivity of AS-K^+ISE sensors of varying K^+ concentrations. The AS-K^+ISE sensors can detect as low as 0.01 µM of K^+, with a near-Nernstian slope of 59.6 mV per decade within a linear range between 0.1 mM and 100 mM. The lifespan extends to at least 24 weeks, with instantaneous response of 3-10 s toward increasing K^+ concentrations. The AS-K^+ISE sensors showed a superior selectivity toward K^+ over interfering ions Na^+, and was successfully evaluated to detect varying K^+ concentrations in aqueous media. Finally, the ability of the developed AS-K^+ISE sensors was validated by monitoring dynamic K^+ changes in aedes mosquito larvae. The results demonstrated performance of all-solid-state sensors based on screen printed electrodes that have performance of sensitivity, selectivity, and lifetime compared to microfabricated electrodes, paving efforts towards a low cost with high performance sensors for biomedical and environmental applications.

خلاصة البحث

تعتبر مستشعرات الأقطاب الكهربية الانتقائية للأيونات (ISE) خيارًا مربحًا للاستخدام في التشخيص الطبي والأمن الغذائي والمراقبة البيئية نظرًا لانخفاض التكلفة وعمليات التصنيع المباشرة. ومع ذلك ، لا تزال المراقبة الفورية للأيونات الفسيولوجية في التشخيص الطبي تمثل تحديًا حيث تعاني أقطاب ISE التقليدية من ضعف الحساسية وحدود الاكتشاف والعمر نظرًا لمحدردية لأغشية الاستشعار في أقطاب ISE التقليدية. تعتبر أقطاب ISE ذات الحالة الصلبة باستعمال أقطاب الكربون المطبوعة (SPCEs) المعدلة احد الحلول. لذالك فان فهم الانعكاس الكهروكيميائي لأداء هذه الاقطاب الصلبة المعدلة ضروري. لذالك قمنا بتعديل أقطاب الكربون المطبوعة (SPCEs) بـ بولي (3،4-إيثيلين ديوكسي ثيوفين) (الصوديوم 4-ستايرين سلفونات) (PEDOT: PSS)، أكسيد الجرافين المرجع المستقر في بوليسترين سلفونات (rGO: PSS) ، ومركب (rGO: PSS-PEDOT: PSS). ثم قمنا بدراسة الخصائص الكهروكيميائية لـ PEDOT: PSS / SPCEs ، و rGO: PSS / SPCEs ، و rGO: PSS-PEDOT: PSS / SPCEs من حيث ذروة التيار (I_p) ، والفرق في ذروة الجهد (ΔE_p) و انزياح في ذروة الجهد (E_{p_shift}) ، وفعالية مساحة السطح (A_e) باستعمال الجهد الدوري (CV). كشفت نتائج قياس الجهد الدوري (CV) لـ rGO: PSS-PEDOT:PSS: ان هناك تأثير تآزري بين PEDOT: PSS و rGO: PSS ، حيث PEDOT: PSS له ذروة تيار عالية (I_p) مما يشير إلى حركية نقل الإلكترون سريعة علي واجهة القطب الكهربائي ، و rGO:PSS له قابلية العكس كما يتضح من E_p و Ep_shift. نظرًا الي ان PEDOT: PSS سجل أعلى ذروة تيار بلغت 1.637 ملي أمبير وهو أعلى بمقدار 23 ضعفًا من rGO:PSS ، قمنا بتصنيع مستشعرات AS-K^+ISE عن طريق وضع غشاء انتقائي للبوتاسيوم (KISM) على المحول PEDOT: PSS / SPCEs. ثم قمنا بقياسات للجهد لتحديد الحساسية ، والانتقائية ، وحد الكشف ، وعمر مجسات القطب الكهربائي الانتقائي لأيون البوتاسيوم (AS-K^+ISE) بتغيير تركيز ايونات البوتاسيوم K^+. وقد اظهرت القياسات ان حد التحسس الادني لـ AS-K^+ISE قد يصل الي 0.01 ميكرومول مع انحدار شبه Nernstian من 59.6 ملي فولط في العقد ضمن نطاق خطي بين 0.1 ملي مول إلى 100 ملي مول. كما امتد العمر الافتراضي للأقطاب إلى 24 أسبوعًا، مع استجابة فورية في 10^{-3} ثوانٍ نحو زيادة تراكيز K^+. كما أظهرت مستشعرات AS-K^+ISE انتقائية فائقة تجاه K^+، وتم اختبارها بنجاح لاكتشاف تركيزات K^+ المتغيرة في الوسائط المائية. أظهرت النتائج المتحصل عليها ان أداء مستشعرات الحالة الصلبة بالكامل بناءً على أقطاب كهربائية مطبوعة على الشاشة تتميز بأداء من الحساسية والانتقائية والعمر يكن مقارنته بالأقطاب الكهربائية الدقيقة ، مما يمهد الجهود نحو تكلفة منخفضة مع أجهزة استشعار عالية الأداء للتطبيقات الطبية والبيئية.

APPROVAL PAGE

I certify that I have supervised and read this study and that in my opinion, it conforms to acceptable standards of scholarly presentation and is fully adequate, in scope and quality, as a thesis for the degree of Master of Science (Electronics Engineering).

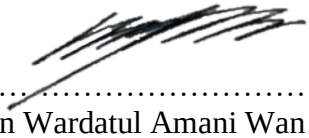

……..
Wan Wardatul Amani Wan Salim
Supervisor

……..
Mohd. Firdaus Abd-Wahab
Co-Supervisor

……..
Mohd Hamzah Mohd Nasir
Co-Supervisor

……..
Noraishah Mydin Abdul Aziz
Field Supervisor

I certify that I have read this study and that in my opinion it conforms to acceptable standards of scholarly presentation and is fully adequate, in scope and quality, as a thesis for the degree of Master of Science (Electronics Engineering).

……..
Nor Farahidah Za'bah
Internal Examiner

……..
Ahmad 'Athif Mohd Fauzi
External Examiner

……..
Anis Nurashikin Nordin
Chairman

This thesis was submitted to the Department of Electrical and Computer Engineering and is accepted as a fulfilment of the requirement for the degree of Master of Science (Electronics Engineering).

……..
Md. Rafiqul Islam
Head, Department of Electrical and Computer Engineering

This thesis was submitted to the Kulliyyah of Engineering and is accepted as a fulfilment of the requirement for the degree of Master of Science (Electronics Engineering).

……..
Sany Izan Ihsan
Dean, Kulliyyah of Engineering

DECLARATION

I hereby declare that this thesis is the result of my own investigations, except where otherwise stated. I also declare that it has not been previously or concurrently submitted as a whole for any other degrees at IIUM or other institutions.

IHDA USWATUN SHALIHAH SHOHIBUDDIN

Signature ..... Date 2/2/2022

INTERNATIONAL ISLAMIC UNIVERSITY MALAYSIA

DECLARATION OF COPYRIGHT AND AFFIRMATION OF FAIR USE OF UNPUBLISHED RESEARCH

ALL-SOLID-STATE ION-SELECTIVE SENSORS FOR MEASUREMENT OF POTASSIUM IONS IN AQUEOUS MEDIA

I declare that the copyright holders of this thesis are jointly owned by the student and IIUM.

Copyright © 2022 Ihda Uswatun Shalihah Binti Shohibuddin and International Islamic University Malaysia. All rights reserved.

No part of this unpublished research may be reproduced, stored in a retrieval system, or transmitted, in any form or by any means, electronic, mechanical, photocopying, recording or otherwise without prior written permission of the copyright holder except as provided below:

1. Any material contained in or derived from this unpublished research may be used by others in their writing with due acknowledgement.

2. IIUM or its library will have the right to make and transmit copies (print or electronic) for institutional and academic purposes.

3. The IIUM library will have the right to make, store in a retrieved system and supply copies of this unpublished research if requested by other universities and research libraries.

By signing this form, I acknowledged that I have read and understand the IIUM Intellectual Property Right and Commercialization policy.

Affirmed by Ihda Uswatun Shalihah Binti Shohibuddin.

…….…….. 2/2/2022 ……..

Signature Date

ACKNOWLEDGEMENTS

إن الحمد لله ونستعينه ونستغفره، ونعوذ بالله من شرور أنفسنا ومن سيئات أعمالنا، من يهده الله فلا مضل له ومن يضلل فلا هادي له، وأشهد أن لا إله إلا الله وحده لا شريك له، وأشهد أن محمدا عبده ورسوله.

اللهم صل على سيدنا محمد الفاتح لما أغلق، والخاتم لما سبق، ناصر الحق بالحق، والهادي إلى صراطك المستقيم، وعلى آله وصحبه حق قدره ومقداره العظيم. اللهم صل على سيدنا محمد خير البرية صلاة ترضيك وترضيه وترضي بها عنا يا رب العالمين. أما بعد.

I thank Allah SWT for giving me the opportunity and strength to complete this thesis. He is the Most Powerful, the Most Helpful, and the main source of my inner strength that makes me to keep going. In addition, my journey throughout the project could not have reached a success without the tremendous support and encouragement I received from numerous individuals and institutions.

Firstly, I would like to express my sincerest gratitude to Assoc. Prof. Dr. Wan Wardatul Amani Wan Salim, my supervisor from Kulliyyah of Engineering, who despite of being extraordinarily busy with her mission and duties, she still spends her time to guide, motivate, and keep me on the correct path to achieve my goals. Her practical viewpoints on problems have opened new inroads for me in tackling many research obstacles. She has exposed me to not only in studies but trained me to be a young professional woman in the future. Thank you for always being patient and pushing me beyond the limit that I never imagined before. I would not have been able to accomplish this work without her efforts.

My deepest appreciation goes to my lovely family; to my mother, Siti Mursyidah Abdul Djalil, a strong and gentle soul, the bravest woman, for her love,

patience, affection, and prayers of day and night. I wish one day I can fulfill the hopes that she has placed in me inshaAllah. To my father, Shohibuddin Laming, my first hero, who has always been proud of me, encouraged me to go forward and be ambitious. To my dear siblings; Wafa Abdul Jabbar, Salmiyah Nurunniyah, Hindah Khairiyah, Zainab Nurul Izzah, and Niswah Zinnirah. Thank you for the unconditional support, pray, and love that has made this thesis both possible and meaningful.

A bouquet of thanks also goes to the academicians of Kulliyyah of Engineering especially from the Department of Electrical and Computer Engineering and the Department of Biotechnology Engineering for their support and help. I also wish to express my appreciation to my co-supervisors; Prof. Dr. Anis Nurashikin Nordin, Asst. Prof. Dr. Mohd Firdaus Abd-Wahab, Asst. Prof. Dr. Mohd Hamzah Mohd Nasir, and Asst. Prof. Dr. Noraishah Mydin Abdul Aziz for their support, ideas, and resources to aid me completing this thesis.

A special thanks to Amani Research Group (ARG) colleagues; to Sr. Nasteho Ali who was the first accompanied me in the lab and showed me to do activation of screen-printed electrodes, to Br. Benoudjit AbdelMohsen who taught me the electropolymerization of PEDOT:PSS, and to Br. Piravin Raj Barthasarathy who always support me throughout the life between studies and works. Not forgotten to my ex-roommates: Huda, Xiao Yu, Aisyah, Aida, and Afifah, thank you for the cherish and enjoyable moment we had throughout our studies.

Last but not the least, a sincere gratitude and appreciation to nanoSkunkWorkX Sdn Bhd who funded and make this project into a reality.

TABLE OF CONTENTS

Abstract ……..… iii
Abstract in Arabic ……. iv
Approval Page …… v
Declaration ……... vii
Copyright Page …… viii
Acknowledgements ……ix
Table of Contents ……..… xi
List of Tables ..……..…. xvii
List of Figures ……...……. xvii
List of Abbreviations ……..… xvii
List of Symbols …… xxvi
List of Units …… xxvii

CHAPTER ONE: INTRODUCTION 1
1.1 Introduction 1
1.1.1 Overview of Sensor Technologies 1
1.1.2 Ion-Selective Electrodes for Ion Measurements in Physiology ... 3
1.2 Research Motivation and Significance 5
1.3 Problem Statement 5
1.4 Research Objectives 7
1.5 Research Scope 8
1.6 Thesis Organisation 9

CHAPTER TWO: LITERATURE REVIEW 11
2.1 Fundamental Concept of Ion Selective Electrodes 11
2.1.1 Ion Selective Electrodes (ISEs) 11
2.1.2 Potassium-Ion Selective Electrode (K^+ISE) Sensors 17
2.2 Commercial K^+ISE Sensors Available in the Market 18
2.3 Potassium Ion-Selective Membrane as the Recognition Component of Ion-Selective Electrodes 22
2.3.1 Valinomycin and Mutacin as Potassium Ionophores 24
2.3.2 Ionic Additives as Lipophilic Salt 24
2.3.3 Plasticizer as Membrane Solvent 25
2.3.4 Polymer Matrix 25
2.4 Transducer Development for Potassium Ion-Selective Electrodes 28
2.4.1 Conventional K^+ISE Sensors 28
2.4.2 All-Solid-State Potassium Ion-Selective Electrode (AS-K^+ISE) Sensors 28
2.5 Nanomaterial-Based All-Solid-State Transducers for an Improved Sensitivity of AS-K^+ISE Sensors 29
2.5.1 Poly(3,4-ethylenedioxythiophene) polystyrene sulfonate (PEDOT:PSS) 29
2.5.2 Graphene as Nanomaterials 32

2.5.3 Graphene Oxide (GO) and Partially Reduced Graphene Oxide (prGO) 33
2.6 Comparison of Substrates, Transducers, and Recognition Components Used by Previous Studies and the Research Gap for the Development of the AS- K^+ISE Sensors 35
2.7 Chapter Summary 39

CHAPTER THREE: EXPERIMENTAL METHODS 40
3.1 Instrument, Reagents, and Materials 44
3.1.1 Instrument 44
3.1.2 Reagents and Materials 45
3.2 Fabrication of Drop-Cast and Electropolymerized rGO:PSS-PEDOT:PSS/SPCEs 47
3.2.1 Activation of Screen-Printed Carbon Electrodes 47
3.2.2 Deposition of rGO:PSS-PEDOT:PSS composite on SPCEs 47
3.2.3 Surface Morphology of rGO:PSS-PEDOT:PSS/SPCEs using Scanning Electron Microscopy 49
3.3 Cyclic voltammetry (CV) Analysis 49
3.3.1 CV Analysis of Electropolymerized and Drop-Cast rGO:PSS-PEDOT:PSS/SPCEs 49
3.3.2 CV Analysis of PEDOT:PSS/SPCEs, rGO:PSS/SPCEs, and rGO:PSS-PEDOT:PSS/SPCEs 50
3.3.3 CV Parameters for Characterization of PEDOT:PSS/SPCEs, rGO:PSS/SPCEs, and rGO:PSS-PEDOT:PSS/SPCEs 51
3.3.4 Significance Test Using "R" Software 52
3.4 Spectral Fingerprints Analyses 53
3.4.1 Fourier Transform Infrared Spectroscopy (FTIR) 53
3.4.2 Raman Spectroscopy 53
3.5 Development of All-Solid-State Potassium Ion-Selective Electrode (AS-K^+ISE) Sensors 54
3.5.1 Characterization of KISM with PEDOT:PSS, rGO:PSS, and rGO:PSS-PEDOT:PSS as Ion-to-Electron Transducers 54
3.5.2 Preparation of K^+ Sensing Membrane 54
3.5.3 Fabrication of AS-K^+ISE Sensors 55
3.6 Potentiometry and Calibration Curve of AS-K^+ISE Sensors 58
3.7 Sensor Performance Analysis of AS-K^+ISE Sensors 59
3.7.1 Sensitivity 59
3.7.2 Linear Range and Response Time 60
3.7.3 Selectivity 61
3.7.4 Limit of Detection 62
3.7.5 Lifetime 63
3.8 Validation of AS-K^+ISE Sensors by Monitoring Extracellular K^+ Levels in Aedes Mosquito Larvae 63
3.9 Morphological Analyses of KISM using Scanning Electron Microscopy 66
3.10 Chapter Summary 66

CHAPTER FOUR: RESULTS AND DISCUSSION **67**
4.1 Introduction 67
4.2 Fabrication of Electropolymerized and Drop-Cast rGO:PSS-PEDOT:PSS/SPCEs 68
4.2.1 Activation of SPCEs 68
4.2.2 Deposition of rGO:PSS-PEDOT:PSS on SPCEs 69
4.2.3 Surface Morphology of rGO:PSS-PEDOT:PSS/SPCEs using Scanning Electron Microscopy 71
4.3 Cyclic Voltammetry (CV) Analysis 73
4.3.1 CV Analysis of Electropolymerized and Drop-Cast rGO:PSS-PEDOT:PSS/SPCEs 73
4.3.2 CV Analysis of PEDOT:PSS/SPCEs, rGO:PSS/SPCEs, and rGO:PSS-PEDOT:PSS/SPCEs 76
4.3.3 Significance Test Using "R" Software 87
4.4 Spectral Fingerprint Analysis 87
4.4.1 Fourier Transform Infrared Spectroscopy (FTIR) 87
4.4.2 Raman Spectroscopy 89
4.5 Development of All-Solid-State Potassium Ion-Selective Electrode (AS-K^+ISE) Sensors 92
4.5.1 Characterization of KISM with PEDOT:PSS, rGO:PSS, and rGO:PSS-PEDOT:PSS as Ion-to-Electron Transducers 92
4.5.2 Fabrication of AS-K^+ISE Sensors 94
4.6 Potentiometry and Calibration Curve of AS-K^+ISE Sensors 96
4.7 Sensor Performance Analysis 99
4.7.1 Selectivity and Specificity of AS-K^+ISE Sensors Towards K^+ with the Presence of Non-Target Analytes 99
4.7.2 Limit of Detection of AS-K^+ISE Sensors 102
4.7.3 Lifetime of AS-K^+ISE Sensors 103
4.7.4 Comparison of Sensor Performance of the Developed AS-K^+ISE Sensors with Other Potassium Sensors from Previous Studies 105
4.8 Validation of AS-K^+ISE Sensors by Monitoring Extracellular K^+ Levels in Aedes Mosquito Larvae 111
4.9 Surface Morphology of KISM/SPCEs Before and After Potentiometry Measurements 115
4.10 Concluding Remarks 118

CHAPTER FIVE: CONCLUSION AND FUTURE WORK **119**
5.1 Conclusion 119
5.2 Outlook and Future Work 121

REFERENCES **123**

LIST OF PUBLICATIONS AND POSTER PRESENTATIONS **136**

APPENDIX **140**
A.1 Materials and CAS Numbers 140
A.2 Calculating wt% 141
A.3 Influence of Supporting Electrolytes on Electrochemical Reversibility of rGO:PSS and rGO:PSS-PEDOT:PSS 142
A.4 Monitoring Extracellular K^+ Levels in Aedes Mosquito Larvae 143
A.5 Potentiometry Measurements Table 144
A.6 Experiments and Labworks Setup 147
A.7 Coding Using "R" Software 153
A.7.1 Significance Test 153
A.7.2 Plot Cyclic Voltammograms 161

LIST OF TABLES

Table 2.1: Summary of the available commercial K^+ISE sensors with their application, sensitivity, linear range, and LOD characteristics. 20

Table 2.2: Composition of potassium ion-selective membrane (KISM) with their % w/w. 23

Table 2.3: The substrate, transducer, and recognition components used for the development of AS- K^+ISE sensors together with their applications. GCE: glassy carbon electrodes; PET: polyethylene terephthalate; PEDOT:PSS: poly(3,4-ethylenedioxythiophene):poly (styrenesulfonate); G/PEDOT:PSS: graphene-poly(3,4-ethylenedioxythiophene):poly(styrenesulfonate) composite; POT: poly(3-octylthiophene-2-5-diyl); MWCNT: multi-wall carbon nanotubes; MOF: metal-organic frameworks; PVC: polyvinylchloride; KTCPB: potassium tetrakis(chlorophenyl)borate; KTFPB: potassium tetrakis[3,5-bis(trifluoromethyl)phenyl]borate; NaTFPB: sodium tetrakis[3,5-bis(trifluoromethyl)phenyl]borate; *o*-NPOE: *o*-nitrophenyloctylether; DOS: bis(2-ethylhexyl) sebacate; THF: tetrahydrofuran; ns: not specified. 36

Table 3.1: Activation input parameters using IVIUM software. 47

Table 3.2: The deposition parameters setup using electropolymerization methods. 48

Table 3.3: Parameters set using IVIUM software for electrochemical characterization using cyclic voltammetry. 50

Table 3.4: The input parameters for potentiometric measurements using IVIUM software. 58

Table 4.1: Peak current (I_p), effective surface area (A_e), and peak-to-peak potential separation (ΔE_p) of bare SPCEs, electropolymerized, and drop-cast rGO:PSS-PEDOT:PSS/SPCEs. CV: cyclic voltammetry; SPCEs: screen-printed carbon electrodes; EPD: electropolymerized rGO:PSS-PEDOT:PSS/SPCEs; DC: drop-cast rGO:PSS-PEDOT:PSS/SPCEs. The results show that the DC produced higher I_p and larger A_e compared to EPD and SPCEs, whereas EPD has lower ΔE_p than DC (blue highlights). 73

Table 4.2: The I_{pa} of SPCEs, PEDOT:PSS/SPCEs, rGO:PSS/SPCEs, and rGO:PSS-PEDOT:PSS/SPCEs. 76

Table 4.3: The E_{p_shift} of SPCEs, PEDOT:PSS/SPCEs, rGO:PSS/SPCEs, and rGO:PSS-PEDOT:PSS/SPCEs. 79

Table 4.4: Anodic peak current (I_{pa}), shift in peak potentials (E_{p_shift}), and effective surface area (A_e) of bare SPCEs, PEDOT:PSS/SPCEs, rGO:PSS/SPCEs, and rGO:PSS-PEDOT:PSS/SPCEs. The results reveal that PEDOT:PSS/SPCEs have higher I_p and larger A_e compared to SPCEs and rGO:PSS/SPCEs (blue highlights). 80

Table 4.5: The sensitivity of the electrodes modified with KISM and different transducer materials towards varying K^+ concentrations. The Nernstian-response of AS-K^+ISE sensors is 59.0 mV/decade. 92

Table 4.6: The sensor performance of the AS-K^+ISE sensors (KISM/PEDOT:PSS/SPCEs) compared to KISM/SPCEs and PEDOT:PSS/SPCEs. 96

Table 4.7: Overall sensing performance of several other potassium sensors from previous literature in comparison to this study. PEDOT:PSS: poly(3,4-ethylenedioxythiophene): poly(styrenesulfonate); GCE: glassy-carbon electrodes; PET: polyethylene terephthalate; PEN: polyethylene naphthalate; G/PEDOT:PSS: graphene-poly(3,4-ethylenedioxythiophene):poly(styrenesulfonate) composite; POT: poly(3-octylthiophene-2-5-diyl); MWCNT: multi-wall carbon nanotubes; MOF: metal-organic frameworks; Pt: platinum; Au: gold; SPCEs: screen-printed carbon electrodes; ns: not specified. 107

LIST OF FIGURES

Figure 1.1: Overview of sensor technologies showing potentiometric ISE sensors as a sub-group of electrochemical sensors which is the focus of this study. 2

Figure 2.1: Schematic diagram of a typical potentiometric cell consisting of an ISE and an RE, both are AgCl electrodes immersed in a glass capillary consisting of electrolytes, with the former having ion-selective membrane (ISM) in contact with the sample solution. The RE consists of Ag/AgCl electrodes in a KCl internal reference electrolyte and a salt bridge. The sum of all the boundary potentials (E_1, E_2, E_3, E_4, E_5, E_m, and E_r) is equal to the total potential of the potentiometric cell. Ions i and j are the target and interfering ions, respectively. ISE: ion-selective electrode. ISM: ion-selective membrane. RE: reference electrode. Ag/AgCl: silver/silver chloride. KCl: potassium chloride. 12

Figure 2.2: Historical background and the progress of nanotechnology in ISEs field and ultimately my contribution in this field. The methods of ion measurement started as early as 1930s, but using conventional liquid-based ISEs, before the emergence of all-solid-state ISEs in 1971. The ion measurement continued with the advancement of ELISA, ion chromatography, and atomic absorption spectroscopy. However, these methods are laborious and time-consuming. The emergence of nanotechnology – conductive polymers was found in late 1980s and graphene in 2005 – has opened a new path in inventions and innovations. Real-time Ca^{2+} measurement was conducted using SporeSAT in 2014 where the NASA team studied polarization of Ca^{2+} due to microgravity while the sensors were orbiting in the space. ISEs have been also proposed for continuous water monitoring using MobiSENS as a portable sensor. My contribution in this field is in the development of ISEs using nanotechnology for K^+ measurement in aqueous media, which can be applied for physiological sensing. 16

Figure 2.3: Previous works done on detecting specific ions of interest using ion-selective electrodes (ISEs). In this study, we will focus on ISEs for monovalent cations detection and quantification using potassium ion-selective electrode (K^+ISE) sensors. The development of K^+ISE sensors is important because K^+ is a major ion-species in the function of human

body and plays a major role in physiological functions. Thus, the concentration of K^+ must be carefully monitored and maintained. 18

Figure 2.4: Schematic representation of (a) 2D, (b) 3D, and (c) space-fill models of mutacin, KTCPB, *o*-NPOE, and PVC for potassium-selective membrane drawn using *ACD/ChemSketch* software. The 2D model shows that the positively charged K^+ attracts with negatively charged B^- in KTCPB. Single and double bonds of the potassium ion-selective membrane (KISM) components were also shown. The 3D model illustrates the arrangement of carbon (turquoise), oxygen (red), and sulfur (yellow), hydrogen (white), and chloride (green) atoms and potassium ions (dark blue) of KISM components. The space-fill model informs the radii of each atom. The big dark blue ion is the K^+ of KTCPB. KTCPB: Potassium tetrakis(4-chlorophenyl)borate; *o*-NPOE: *o*-nitrophenyl octyl ether; PVC: polyvinylchloride. 27

Figure 2.5: Schematic representation of (a) 2D, (b) 3D, and (c) space-fill models of conductive polymer PEDOT:PSS using *ACD/ChemSketch* software. The 2D model shows that the positively charged S^+ of PEDOT backbone interacts with negatively charged O^- of PSS chain, shown by the dotted line. Single and double bonds of PEDOT:PSS were also shown. The 3D model illustrates the arrangement of carbon (turquoise), oxygen (red), and sulfur (yellow) atoms of PEDOT:PSS structure. The space-fill model informs us the radii of each atom. 31

Figure 2.6: The schematic representation of graphene and its derivatives. The 2D structures of (a) graphene, (b) graphene oxide and (c) partially reduced graphene oxide (edited from Georgakilas et al., 2016). (d) and their comparisons of conductivity and hydrophobicity. 34

Figure 3.1: The flow chart of the research methodology performed by this study. 42

Figure 3.2: (a) Photographic image of SPCEs showing the dimension in comparison to a 20-cent coin. (b) magnification of working, counter, and reference electrodes using Leica images; the reference electrode is 1 mm in diameter. (c) magnification of working electrode (WE) using Leica images; the WE is 2 mm in diameter, almost one tenth of the diameter of the 20-cent coin. 45

Figure 3.3: Schematic of the components of AS-K^+ISE sensors. **(a)** Screen-printed carbon electrodes (SPCEs) drop-cast with PEDOT:PSS transducer and ion-selective membrane for K^+

(KISM), showing the chemical structures of transducers PEDOT:PSS and mutacin-based KISM; four main components of KISM which includes PVC, *o*-NPOE, KTC|PB, and mutacin. **(b)** Illustration of the interactions between the mutacin-based ionophore and K^+/Na^+ in bulk solution. K^+ interacts with the mutacin at the KISM surface, which makes the sensing layer energetically favorable for K^+ to pass through the KISM; however, smaller Na^+ cannot fully interact with the oxygen atoms of the KISM, thus, Na^+ is less attractive to the KISM and repels from the KISM surface. The flow of electrons generated from transducer to electronic components was also shown. K^+ detected by the mutacin are carried to transducers. Conductive polymers PEDOT doped with PSS react with K^+ which generate electrons. The electrons are then measured and quantified by a potentiostat and signals are displayed using IVIUM software. **(c)** Interactions of PEDOT:PSS with K^+ as the target ions, and the generations of electrons. **(d)** Analysis performed in this study: cyclic voltammetry (CV) and potentiometry. CVs are performed to characterize transducers by understanding the peak current, I_p, peak potential, E_p, and effective surface area, A_e. Potentiometry is conducted to analyze the sensors performance which includes sensitivity, linear range, response time, selectivity, limit of detection, and lifetime. 57

Figure 3.4: A linear curve of a response against analyte concentration. The slope of the linear curve represents the sensitivity of AS-K^+ISE sensors. Larger slope indicates higher sensitivity. 60

Figure 3.5: Experimental setup of monitoring extracellular K^+ levels in solutions, with and without aedes mosquito larvae, using AS-K^+ISE sensors. 65

Figure 4.1: Cyclic voltammogram of activation process of SPCEs using IVIUM software. The potential was scanned at extreme anodic (2.5 V) and cathodic potentials (-2.5 V) for 3 cycles at a scan rate of 100 mV/s in 0.1 N sulfuric acid (H_2SO_4) solution. The inset is the cyclic voltammogram from the manual of PINE Research Instrumentation, (Screen-printed, 2019) which confirmed the successful activation of the SPCEs conducted in this study. 69

Figure 4.2: The Leica Microscope image of (a) bare SPCEs, (b) electropolymerized and (c) drop-cast rGO:PSS-PEDOT:PSS/SPCEs. In comparison to bare SPCEs as control, the microscope images confirmed the deposition of electropolymerized and drop-cast rGO:PSS-PEDOT:PSS on the WE of SPCEs. 71

Figure 4.3: Surface morphology of (**a**) bare SPCEs, (**b**) electropolymerized rGO:PSS-PEDOT:PSS/SPCEs, and (**c**) drop-cast rGO:PSS-PEDOT:PSS/SPCEs. Bare SPCEs display an original crumbled surface with flaky design and rippled edged, paper-like sheet structures. Once the working electrode (WE) of the bare SPCEs was modified using electropolymerized rGO:PSS-PEDOT:PSS, the SEM micrographs show that the surface of the WE is homogeneously covered by tightly distributed globular structures. Detailed analysis using Image J software reveal that the globule diameters are in the range of 1.4 – 5.3 µm. Meanwhile, drop-cast rGO:PSS-PEDOT:PSS/SPCEs show some valley-like and bumps structures with tiny grains. 72

Figure 4.4: (**a**) Cyclic voltammetry (CV) measurements of bare SPCEs, electropolymerized and drop-cast rGO:PSS-PEDOT:PSS/SPCEs at a scan rate of 100 mV/s in 0.1 M $K_3Fe(CN)_6$. ΔI_p is shown. Around 5-fold increase in ΔI_p from 0.168 mA for $\Delta I_{EPD\text{-}Bare}$ to 0.798 mA for $\Delta I_{DC\text{-}Bare}$. CV measurements of (**b**) SPCEs, (**c**) drop-cast rGO:PSS-PEDOT:PSS/SPCEs, and (**d**) electropolymerized rGO:PSS-PEDOT:PSS/SPCEs at scan rates of 75, 100, 150, 200, 250 mV/s in 0.1 M $K_3Fe(CN)_6$. ΔE_p is shown. The electropolymerized rGO:PSS-PEDOT:PSS/SPCEs showed a lower ΔE_p of 360 mV, 1.4 times lower than those of drop-cast rGO:PSS-PEDOT:PSS/SPCEs (ΔE_p = 510 mV). 75

Figure 4.5: (a) Cyclic voltammetry (CV) measurements of PEDOT:PSS/SPCEs, rGO:PSS/SPCEs, and rGO:PSS-PEDOT:PSS/SPCEs at a scan rate of 100 mV/s in 0.1 M $K_3Fe(CN)_6$. ΔI_p was shown in the CV graphs. (b) CV measurements of rGO:PSS/SPCEs at scan rates of 75, 100, 150, 200, and 250 mV/s. ΔE_p and E_{p_shift} were shown. (c) Bar graphs showing I_{pa} and E_{p_shift} for SPCEs, rGO:PSS/SPCEs, PEDOT:PSS/SPCEs, and rGO:PSS-PEDOT:PSS/SPCEs. Transducer rGO:PSS-PEDOT:PSS revealed synergistic effect of rGO:PSS and PEDOT:PSS composite where rGO:PSS is highly reversible as evidenced by the small shift in E_{p_shift} and PEDOT:PSS has a high I_p suggesting more electron transfer at the electrode-electrolyte interface. (d) Effective surface area, A_e, was determined using the slope and the Randles-Sevcik equation. Results show that PEDOT:PSS and rGO:PSS-PEDOT:PSS improved the A_e with 13.7 mm^2 and 6.7 mm^2, respectively, compared to SPCEs of 3.1 mm^2. The experimental A_e value of SPCEs confirmed the theoretical area of working electrode which was 3.14 mm^2. 81

Figure 4.6: Cyclic voltammetry of (a) PEDOT:PSS/SPCEs, (b) rGO:PSS/SPCEs, and (c) rGO:PSS-PEDOT:PSS/SPCEs in 0.1 M $K_3Fe(CN)_6$ with the presence (blue) or absence (black)

of 1 M KCl at a scan rate of 200 mV/S. A higher I_p was observed when DMSO was mixed to rGO:PSS, indicating DMSO improves the electrical conductivity of rGO:PSS/SPCEs. 85

Figure 4.7: Cyclic voltammetry of PEDOT:PSS/SPCEs at a scan rate 100 mV/s. ΔE_p is shown. The red arrows show the scanning direction. The blue and black lines represent CV measurements in the presence and absence of 1 M KCl as a supporting electrolyte, respectively. A smaller ΔE_p was produced when incorporating KCl, which implies supporting electrolyte reduced migration effects. 87

Figure 4.8: Spectral fingerprint analysis using fourier transform infrared spectroscopy (FTIR). 89

Figure 4.9: Raman spectra of bare SPCEs, rGO:PSS/SPCEs, PEDOT:PSS/SPCEs, and rGO:PSS-PEDOT:PSS/SPCEs recorded using the 785 nm laser excitation, over a wavelength range of 100 to 2100 cm^{-1}. 91

Figure 4.10: **(a)** Potentiometric measurement of KISM/rGO:PSS/SPCEs, KISM/PEDOT:PSS/SPCEs, and KISM/rGO:PSS-PEDOT:PSS/SPCEs. (b) Calibration profile for KISM/rGO:PSS/SPCEs, KISM/PEDOT:PSS/SPCEs, and KISM/rGO:PSS-PEDOT:PSS/SPCEs in KCl with increasing concentration from 0.1, 1, 2, 4, 8, 16, 32, 100, and 1000 mM. The KISM/PEDOT:PSS/SPCEs indicates a near-Nernstian responses of 59.6 mV/decade, which is close to the theoretical Nernstian value of K^+ISE sensors (59 mV/decade). A super-Nernstian response of 68.4 mV/decade was observed for KISM/rGO:PSS/SPCEs. The inclusion of PEDOT:PSS to the rGO:PSS made the KISM/rGO:PSS-PEDOT:PSS/SPCEs 31.9 % closer to Nernstian response when compared to the KISM/rGO:PSS/SPCEs. 94

Figure 4.11: **(a)** Potentiometry measurement of KISM/SPCEs, PEDOT:PSS/SPCEs, and KISM/PEDOT:PSS/SPCEs. **(b)** Calibration profile for KISM/SPCEs, PEDOT:PSS/SPCEs, and KISM/PEDOT:PSS/SPCEs. A linear relationship between voltage and K^+ concentration with sensitivity of 52.8 mV/decade for PEDOT:PSS/SPCEs was observed, which increased to 59.6 mV/decade for KISM/PEDOT:PSS/SPCEs, and further increased to 64.7 mV/decade for KISM/SPCEs. The results suggest that transducer layers play an important role in stabilizing the voltage; as an ion-to-electron transducer of AS-ISEs, with negligible voltage drift. Meanwhile KISM is responsible for selectively detecting target ions and allows a specific capturing of K^+, hence more ions are transduced into electrons, thus improving the voltage signals. 98

Figure 4.12: Selective K^+ detection and real-time monitoring of AS-K^+ISE sensors against a physiological non-target analyte, Na^+. (a) Separate Solution Method. A negligible or small interference of 2 - 6 mV voltage change was observed in NaCl, compared to 20 - 45 mV voltage change in KCl. (b) Fixed Interference Method. The lowest detection limit of KCl was determined in 77 mM of background solution NaCl. KCl was detected as low as 0.1 mM in 77 mM NaCl. A weak interference of Na^+ of log $K_{K,Na}$ = -2.9 was observed, suitable for monitoring a low amount of K^+ in the presence of high Na^+. This indicates the superior K^+ selectivity of the AS-K^+ISE sensors attributed to the KISM that excludes passage of interfering ions. 101

Figure 4.13: The detection limit of AS-K^+ISE sensors towards K^+ was determined by performing potentiometry at concentrations as low as 10^{-5} to 100 mM. **(a)** Voltage changes of AS-K^+ISE sensors were observed and measured as the KCl concentrations increased from 10^{-5} to 100 mM in DI water. Results suggest that K^+ was detected as low as 0.01 µM. **(b)** Calibration curve for AS-K^+ISE sensors in KCl with increasing concentrations from 10^{-5} to 100 mM. Results indicate that the linear range was from 0.1 mM to 100 mM, suitable for K^+ physiological concentration range of 4 - 100 mM. 103

Figure 4.14: Lifetime of the AS-K^+ISE sensors was studied. Potentiometric measurements in **(a)** the first and **(b)** the sixth months after fabrication of the AS-K^+ISE sensors. KCl of concentrations 0.1, 1, 2, 4, 8, 16, and 32, 100, and 1000 mM were dropped into a glass vial containing 11 ml DI water. Voltage changes were observed. The AS-K^+ISE sensors were then sealed by parafilm to avoid moisture and contamination and were stored in the dark. Same measurements were repeated after 6 months using the same AS-K^+ISE sensors. Steps were seen in both potentiometric graphs, suggesting that the AS-K^+ISE sensors can have lifetime capability and potentiometric measurements stability after 6 months. Calibration curve of the AS-K^+ISE sensors in **(c)** the first and **(d)** the sixth months after fabrications. The linear range remained almost the same for both potentiometric measurements with 0.042 - 3.3 mM in the first month, and 0.080 - 3.3 mM in the sixth month. The R^2 reduced by only 0.0071, where R^2 = 0.9974 and R^2 = 0.9903 for the AS-K^+ISE sensors in the first and sixth months, respectively. The results indicate lifetime capability of the AS-K^+ISE sensors after six months of storage. 105

Figure 4.15: The extracellular K^+ levels of Aegypt and Albopratas measured by the AS-K^+ISE sensors. DI water was measured as a negative control. Real-time potentiometry measurements

of solutions containing Aegypt and Albopratas revealed a trend of increasing and decreasing K^+ concentrations, respectively, throughout measurements of 6000 s (1 hour 40 minutes). In contrast, DI water shows a clean, constant, and stable extracellular K^+ levels throughout the same time frame of 6000 s. 112

Figure 4.16: The extracellular K^+ levels in solutions, with and without (a) Aegypt and (b) Albopratas, aedes mosquito larvae measured by the AS-K^+ISE sensors. The solutions without the larvae and solutions in DI water were measured as negative controls. (a) The trend of extracellular K^+ levels in solutions without Aegypt followed the trend of those in DI water, where both cases reached a stable voltage at around t = 1000 s. On the contrary, the extracellular K^+ levels in solutions with Aegypt revealed a trend of increasing K^+ concentrations at a slower rate compared to those without Aegypt, where the voltage reached stability at t = 3000 s. (b) The same trend of extracellular K^+ levels of stable voltage signals was observed in both solutions without Albopratas and DI water throughout the 6000 s. On the contrary, the extracellular K^+ levels in solutions with Albopratas revealed a trend of decreasing K^+ concentrations from 800 mV to 740 mV. 114

Figure 4.17: SEM images of the surface morphology of KISM/SPCEs (**a**) before and (**b**) after potentiometric measurement. The results show the KISM pores open after the potentiometric measurement. Detailed analysis using Image J software reveals that before potentiometric measurement, the pore diameter is in the range of 1.0 - 2.5 µm. However, the pore diameters enlarge up to around 5.0 µm, a two-fold increase after potentiometric measurement. The results suggest that potentiometric measurement affects the opening of ionophore pores which permit only free K^+ to diffuse into and out of the KISM pores. 117

LIST OF ABBREVIATIONS

AS-ISE	All-solid-state ion-selective electrode
AS-K^+ISE	All-solid-state potassium-ion selective electrode
CE	Counter electrode
CV	Cyclic voltammetry
FTIR	Fourier transform infrared spectroscopy
GCEs	Glassy carbon electrodes
GO	Graphene oxide
ISEs	Ion-selective electrodes
ISM	Ion-selective membrane
K^+ISE	Potassium-ion selective electrode
KISM	Potassium-ion selective membrane
KTCPB	Potassium tetrakis(chlorophenyl)borate
LMIC	Low-middle income countries
LOD	Limit of detection
NASA	National aeronautics and space administration
o-NPOE	*o*-nitrophenyloctylether
PEDOT:PSS	Poly(3,4-ethylenedioxythiophene):poly(styrenesulfonate)
POC	Point-of-care
prGO	Partially reduced graphene oxide
PVC	Polyvinylchloride
RE	Reference electrode
rGO	Reduced graphene oxide

rGO:PSS	Reduced graphene oxide stabilized in polystyrenesulfonate
SEM	Scanning electron microscopy
SPCEs	Screen-printed carbon electrodes
SporeSAT	Spore satellite
THF	Tetrahydrofuran